Structural Health Monitoring and Impact Detection Using Neural Networks for Damage Characterization

Richard W. Ross*
NASA Langley Research Center
Hampton, VA 23681-2199, USA

Detection of damage due to foreign object impact is an important factor in the development of new aerospace vehicles. Acoustic waves generated on impact can be detected using a set of piezoelectric transducers, and the location of impact can be determined by triangulation based on the differences in the arrival time of the waves at each of the sensors. These sensors generate electrical signals in response to mechanical motion resulting from the impact as well as from natural vibrations. Due to electrical noise and mechanical vibration, accurately determining these time differentials can be challenging, and even small measurement inaccuracies can lead to significant errors in the computed damage location. Wavelet transforms are used to analyze the signals at multiple levels of detail, allowing the signals resulting from the impact to be isolated from ambient electromechanical noise. Data extracted from these transformed signals are input to an artificial neural network to aid in identifying the moment of impact from the transformed signals. By distinguishing which of the signal components are resultant from the impact and which are characteristic of noise and normal aerodynamic loads, the time differentials as well as the location of damage can be accurately assessed. The combination of wavelet transformations and neural network processing results in an efficient and accurate approach for passive in-flight detection of foreign object damage.

Nomenclature

f	=	signal represented in the time domain
F	=	signal represented in the frequency domain
T	=	time
$W(a,b)$	=	wavelet transform coefficients
ψ	=	wavelet basis function
ψ^*	=	complex conjugate of wavelet function
$\psi_{a,b}$	=	wavelet function (scaled and time shifted)
ω	=	frequency

I. Introduction

THE on-board, near real-time detection of foreign object impacts, and the assessment of their potential to lead to structural damage, is becoming an increasingly important consideration in the development of new aerospace vehicles. While damage detection was once largely the domain of ground-based pre- and post flight inspections in a controlled environment, incidents such as the catastrophic failure of the space shuttle Columbia in February 2003 during reentry and numerous aviation accidents resulting from foreign object damage have spurred the need for *in-situ* damage detection and impact detection methods.[1]

Piezoelectric transducers are often the sensor of choice for in-flight impact detection because of their low cost and their ability to operate either in an active or in a passive mode.[2] Acoustic waves generated on impact can be detected using a set of four piezoelectric transducers, and the location of impact can be determined by triangulation based on the differences in the arrival time of the waves at each of the piezoelectric sensors. These sensors generate electrical signals in response to mechanical motion resulting from the impact as well as from natural vibrations. Due

* Aerospace Engineer, Mechanics of Structures and Materials Branch, MS 188E, Member AIAA.

to electrical noise and mechanical vibration, accurately determining these time differentials can be challenging, and even small measurement inaccuracies can lead to significant errors in the computed damage location.[3]

Wavelet transforms are used to analyze the signals at multiple levels of detail to distinguish them from ambient electromechanical noise. Wavelet transforms have often been demonstrated to be more beneficial than other signal processing methods since they simultaneous retain the characteristics of the original signal in both the time and the frequency domains.

Data extracted from these transformed signals are input to an artificial neural network to aid in identifying the region of interest (that is, the moment of impact) from the transformed signals. By distinguishing which of the signal components are resultant from the impact and which are characteristic of noise and normal aerodynamic loads, the time differentials as well as the location of damage can be more accurately assessed. Once properly trained, neural networks are computationally efficient and no iterative calculations are required. Computational efficiency is an important factor for near real time in-flight impact detection because of the reduction in power and weight required for computational hardware. By identifying impacts or other in-flight singularities in a passive mode, more computationally intense damage characterization algorithms using active sensors can be initiated only as needed.

The objective of this paper is to illustrate how a combination of wavelet transforms and artificial neural networks can accurately determine the time differences in the detection of a signal by piezoelectric transducers resulting from an impact, how those time differences can be used to determine the location of that impact, and why accurate determination of these time differences is essential to the accurate location of the impact. This paper shows how wavelet transformations combined with neural network processing results in an effective approach for passive in-flight detection of impacts from foreign objects. After the introduction, the experimental equipment and testing technique is described. In Section III, the triangulation method used to locate the impact site is derived from the differences in the time of the detection of a signal at the piezoelectric transducers, and it shown that the accuracy of the estimated impact site is dependent on the ability to precisely determine the times of arrival of the signal resulting from the impact at each of the sensors. Section IV identifies how wavelet transforms are used to increase the signal to noise ratio in the measured signals. Section V describes how a neural network is employed to identify the time of impact, concluding with the results of this effort in Section VI.

II. Experimental Test Apparatus and Setup

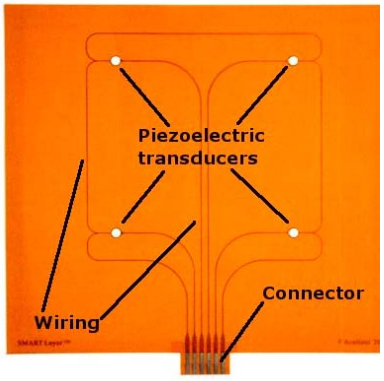

Figure 1. SMART Layer film.

The test experiments were conducted by releasing a 28 g weight from a height of 0.25 m onto a solid planar surface and measuring the resulting acoustic waves generated by impacts at various locations. The surface was 1.5 m x 0.788 m x 18 mm, solidly supported around the perimeter. A commercial product, SMART Layer® from Accellent Technologies, Inc., was used to transform the acoustic waves into electrical signals.[4] The SMART Layer consisted of four piezoelectric transducers arranged in a square pattern, 127 mm on each side, with embedded wiring in a thin dielectric film as shown in Fig. 1.

The piezoelectric transducers were connected to a high-speed data acquisition system which digitized the electrical signal from each sensor and recorded the data. The data acquisition system consisted of a National Instruments PXI-6115 multifunction input/output (I/O) board in a National Instruments PXI-1002 four-slot PXI (PCI (Personal Computer Interface) Extensions for Instrumentation) chassis, shown in Fig. 2. The data acquisition card supported four analog inputs with a dedicated analog to digital converter (ADC) per channel, capable of acquiring a total of 64 megasamples per channel at up to 10 megasamples per second per channel.

Figure 2. National Instruments PXI-1002.

The PXI chassis was connected to a Dell OptiPlex GX270 personal computer via a MXI-4 (Multi-System Extension Interface) to PCI adapter. The data acquisition software used a combination of custom software developed using LabVIEW with NI-DAQ (National Instruments Data Acquisition) software.

The data acquisition card was programmed to trigger when

one of the analog input channel voltages exceeded a threshold, and the trigger level was set to a value slightly above the nominal voltage as measured in a pre-trigger stage. Upon exceeding the threshold level, the software captured and recorded the data to disk. Data from the transducers were sampled at data rates ranging from 200,000 to 10,000,000 samples per second.

A Fourier analysis of the test signals prior to the impact showed dominant noise frequencies of 60 Hz, 20 kHz, and 21.8 kHz (and at their harmonics), in decreasing order of magnitude. After impact, additional frequencies were excited around 160 Hz, 256 Hz, 24 Hz, 13.6 kHz, and 21.3 kHz, in decreasing order of magnitude.

III. Identification of Impact Site

After the data from each piezoelectric transducer have been acquired, the location of the impact can be determined. The impact on the structure causes the piezoelectric elements to react passively to produce an electrical output in response to mechanical vibrations resulting from the impact. As the acoustic wave, radiating in a circular pattern from the source of the impact, reaches each of the four sensors, an electrical signal will be output. Based on the differentials between the times of arrival of the signals at each sensor, the impact location may be determined. The time of initial arrival of the signal at a sensor is used instead of the time of peak value to avoid constructive or destructive wave interference, waves from rebounding impacts, and boundary reflections.[3]

This arrival time is determined in three steps. First, the propagation speed of an acoustic wave through the material is determined. Next, the relative location of the impact is calculated based on the time differentials of the received signals at each of the sensors, and the relative location is transformed into test coordinates to identify the location of the impact. The equations below were derived for custom software implementation using MATLAB® from The MathWorks, Inc.[5]

For materials of uniform density and constant wave propagation speed, this speed can be determined using an experimental calibration technique. By generating a controlled impact at a known location and orientation relative to the sensors, the velocity of a wave through a given material may be determined.

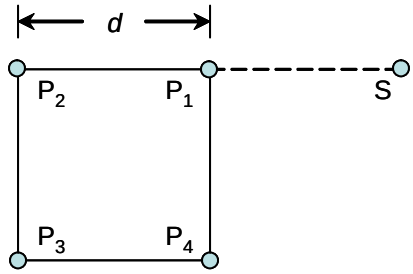

Figure 3. Sensors and impact source.

In Fig. 3, P_1 through P_4 represent the four piezo-electric sensor elements, and S represents the source of impact during calibration. By measuring the time *t* for a signal originating at the source to travel the distance *d* between two sensors, the velocity *d*/*t* of the wave can be computed. To ensure the accuracy of the final result, a high sample rate (10 megasamples per second) was used for measuring the time differentials, and results were averaged from repeated trials.

After the one-time determination of the wave velocity, the location of a foreign object impact can be determined from the time differential between the detection of the impact at each of four sensors. The approach described below is based on a square arrangement shown in Fig. 3 for the four sensors, although other layouts can be used with appropriate coordinate transformations.

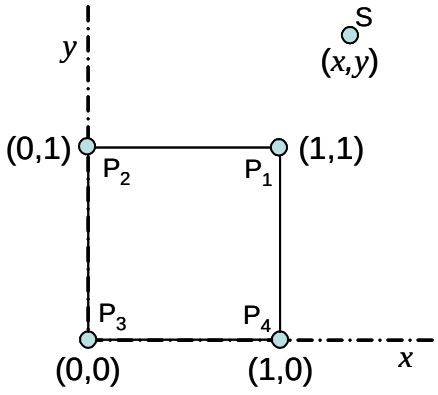

Figure 4. Sensor layout after coordinate transformation.

The wave resulting from the impact was assumed to radiate from a point source and the physical test coordinate system was transformed into a unit square coordinate system using relative positions and distances as shown in Fig. 4. The first sensor to receive the signal is arbitrarily designated as the point P_1 and is located at relative Cartesian coordinates (1, 1). P_2 and P_4 are designated at relative coordinates (0, 1) and (1, 0), respectively. Finally, P_3 is designated at the origin, and the source, *S*, is at an unknown location (*x*, *y*).

With these transformations from test to relative coordinates, the distance between sensors, shown as *d* in Figure 3, becomes unity after transformation to the coordinate system shown in Fig. 4.

For a uniform wave propagation speed, an impact at unknown point *S* outside the boundaries of the sensors radiates outward in all directions and the signal is received at the closest sensor, arbitrarily designated P_1. The signal travels in all directions forming a circle of radius *r*, which is the relative distance from the source, *S*, to sensor P_1, as shown in Fig. 5.

The signal will be received at the remaining three sensors after time lags t_n. These time differentials may be normalized and converted to relative differences using the propagation velocity and actual distance between sensors. The total relative distance traveled by the signal from the source to each of the four sensors, D_n, is the radius of the circle, *r*, plus the remaining distances, d_n, shown in Fig. 5.

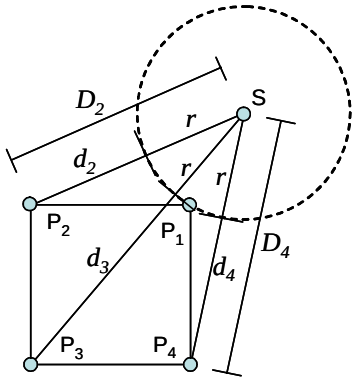

Figure 5. Sensor distances.

Note that for sensor P_1, the total distance, D_1, is merely the radius of the circle, *r*, since t_1 and d_1 are both zero. The three distances can be computed by solving a linear system of simultaneous equations. Once the equations have been solved for these relative distances, the solution can be transformed back to the test coordinates to compute the actual location of the source. Each of these distances can also be expressed as the distance between two points, namely, the distance from the source to the sensor, as shown in Eqs. (1) through (4).

$$D_1 = \|\mathbf{S} - \mathbf{P}_1\| = \sqrt{(x-1)^2 + (y-1)^2} \tag{1}$$

$$D_2 = \|\mathbf{S} - \mathbf{P}_2\| = \sqrt{(x-0)^2 + (y-1)^2} \tag{2}$$

$$D_3 = \|\mathbf{S} - \mathbf{P}_3\| = \sqrt{(x-0)^2 + (y-0)^2} \tag{3}$$

$$D_4 = \|\mathbf{S} - \mathbf{P}_4\| = \sqrt{(x-1)^2 + (y-0)^2} \tag{4}$$

Simplifying and squaring both sides yields Eqs. (5) through (8).

$$D_1^2 = (x-1)^2 + (y-1)^2 = x^2 + y^2 - 2x - 2y + 2 \tag{5}$$

$$D_2^2 = x^2 + (y-1)^2 = x^2 + y^2 - 2y + 1 \tag{6}$$

$$D_3^2 = x^2 + y^2 \tag{7}$$

$$D_4^2 = (x-1)^2 + y^2 = x^2 + y^2 - 2x + 1 \tag{8}$$

The second-order terms in Eqs. (5) through (8) can be eliminated by forming new Eqs. (9) through (11) that are the differences of the original equations.

$$D_1^2 - D_2^2 = 1 - 2x \tag{9}$$

$$D_1^2 - D_3^2 = 2 - 2x - 2y \tag{10}$$

$$D_1^2 - D_4^2 = 1 - 2y \tag{11}$$

From Fig. 5, the total distance D_n is the sum of the radius r plus the remaining distance d_n, so the above equations can be rewritten as Eqs. (12) through (14).

$$1-2x = r^2 - \left(r + d_2\right)^2 = -2d_2 r - d_2^2 \tag{12}$$

$$2-2x-2y = r^2 - \left(r + d_3\right)^2 = -2d_3 r - d_3^2 \tag{13}$$

$$1-2y = r^2 - \left(r + d_4\right)^2 = -2d_4 r - d_4^2 \tag{14}$$

These equations can be rewritten as three equations (Eqs. (15) through (17)) in three unknowns.

$$2x - 2d_2 r = d_2^2 + 1 \tag{15}$$

$$2x + 2y - 2d_3 r = d_3^2 + 2 \tag{16}$$

$$2y - 2d_4 r = d_4^2 + 1 \tag{17}$$

Adding Eqs. (15) and (17), then subtracting Eq. (16), yields the result shown in Eq. (18), which can be solved for r as shown in Eq. (19).

$$2\left(d_3 - d_2 - d_4\right)\cdot r = d_2^2 - d_3^2 + d_4^2 \tag{18}$$

$$r = \frac{d_2^2 - d_3^2 + d_4^2}{2\left(d_3 - d_2 - d_4\right)} \tag{19}$$

Now that the value of r is known, it can be substituted in Equations (15) and (17) and solving for x and y, respectively, which results in Eq. (20) and (21). This system can also be solved using the matrix form in Eq. (22).

$$x = \frac{2d_2 r + d_2^2 + 1}{2} \tag{20}$$

$$y = \frac{2d_4 r + d_4^2 + 1}{2} \tag{21}$$

$$\begin{bmatrix} 2 & 0 & -2d_2 \\ 2 & 2 & -2d_3 \\ 0 & 2 & -2d_4 \end{bmatrix} \cdot \begin{bmatrix} x \\ y \\ r \end{bmatrix} = \begin{bmatrix} d_2^2 + 1 \\ d_3^2 + 2 \\ d_4^2 + 1 \end{bmatrix} \tag{22}$$

The source location previously identified has been defined relative to the unit square coordinate system. These coordinates may be transformed to absolute test coordinates using the transformation given by Eq. (23), where x and y are the relative coordinates, x' and y' are the test coordinates, T_t is the translation matrix, T_s is the scaling matrix, and T_r is the rotation matrices, respectively.

$$\begin{bmatrix} x' \\ y' \\ 1 \end{bmatrix} = T_t \cdot T_s \cdot T_r \begin{bmatrix} x \\ y \\ 1 \end{bmatrix} \tag{23}$$

The translation, scaling, and rotation matrices are all 3x3 matrices, defined as shown in Eqs. (24) through (26), where t_x and t_y are the offsets between the origins of the relative and test coordinate systems, s_x and s_y are scale factors between the two coordinate systems, and θ is the angle between the axes of the coordinate systems.

$$T_t = \begin{bmatrix} 1 & 0 & t_x \\ 0 & 1 & t_y \\ 0 & 0 & 1 \end{bmatrix} \tag{24}$$

$$T_s = \begin{bmatrix} s_x & 0 & 0 \\ 0 & s_y & 0 \\ 0 & 0 & 1 \end{bmatrix} \tag{25}$$

$$T_r = \begin{bmatrix} \cos\theta & -\sin\theta & 0 \\ \sin\theta & \cos\theta & 0 \\ 0 & 0 & 1 \end{bmatrix} \tag{26}$$

These parameters can be derived from the test coordinates of two of the sensors: the first sensor to receive the signal, P_1, and the sensor diagonally across from it, P_3, which is also the origin of the relative coordinate system. The two translation offsets, t_x and t_y, are simply the test coordinates of sensor P_3, so Eq. (24) can be rewritten as shown in Eq. (27), where x_3 and y_3 are the test x and y coordinates of sensor P_3.

$$T_t = \begin{bmatrix} 1 & 0 & x_3 \\ 0 & 1 & y_3 \\ 0 & 0 & 1 \end{bmatrix} \tag{27}$$

The two scale factors, s_x and s_y, are the same as the test length of the sides of the sensor array. The length of one side is easily computed from the distance between P_1 and P_3, which is the length of the diagonal of the square formed by the four sensors, as shown in Eq. (28).

$$s_x = s_y = \sqrt{\frac{(x_1 - x_3)^2 + (y_1 - y_3)^2}{2}} \tag{28}$$

Finally, the test angle between the diagonal formed by P_1 and P_3 is the arctangent of the slope of the diagonal, shown in Eq. (29).

$$\theta = \tan^{-1}\left(\frac{y_1 - y_3}{x_1 - x_3}\right) - \frac{\pi}{4} \tag{29}$$

The term π/4 in Eq. (35) represents the angle of the diagonal, so subtracting this term gives the rotation angle with respect to the *x* axis, not the diagonal. Finally, the three transformation matrices can be multiplied together to form a single transformation matrix, *T*, as shown in Eq. (30).

$$T = T_t \cdot T_s \cdot T = \begin{bmatrix} 1 & 0 & x_3 \\ 0 & 1 & y_3 \\ 0 & 0 & 1 \end{bmatrix} \cdot \begin{bmatrix} s_x & 0 & 0 \\ 0 & s_y & 0 \\ 0 & 0 & 1 \end{bmatrix} \cdot \begin{bmatrix} \cos\theta & -\sin\theta & 0 \\ \sin\theta & \cos\theta & 0 \\ 0 & 0 & 1 \end{bmatrix}$$
$$= \begin{bmatrix} s_x \cos\theta & -s_x \sin\theta & x_3 \\ s_y \sin\theta & s_y \cos\theta & y_3 \\ 0 & 0 & 1 \end{bmatrix} \tag{30}$$

In summary, the relative location of impact can be determined by converting the time differentials to distances (wave propagation velocity divided by time) and by solving Eq. (22) for relative coordinates *x* and *y* plus radius *r*. These relative coordinates can be converted back to physical test coordinates, *x'* and *y'*, using Eqs. (23) and (30).

From Eq. (22) it can be seen that even a small error in the time differential greatly affects the accuracy of the computed *x* and *y* coordinates. For example, consider a damage source arbitrarily located at relative coordinates (2.0, 0.6). The distances corresponding to this location can be determined geometrically using the Pythagorean Theorem (Eq. 31) and Figure 5.

$$d = \sqrt{(x_2 - x_1)^2 + (y_2 - y_1)^2} \tag{31}$$

Using Eq. (31) and Figure 5, the relative distances corresponding to (2.0, 0.6) for d_2, d_3, d_4, and *r* are 1.077, 0.9626, 1.011, and 0.0892, respectively. Using these distances in Eq. (22) correctly results in x and y coordinates of (2.0, 0.6). However, introducing a 1% error in the d_2 term in Eq. (22) results in coordinates of (1.64, 0.57), an 18% error. This error becomes greater with increasing distance between the damage source and the sensors.

IV. Signal Analysis and Wavelet Decomposition

As just shown, accurately determining the location of the impact depends on the precision of the time differentials. Even small discrepancies in the time differential measurements can propagate into significantly larger errors when computing the impact location. Under ideal conditions, there would be no output from the piezoelectric

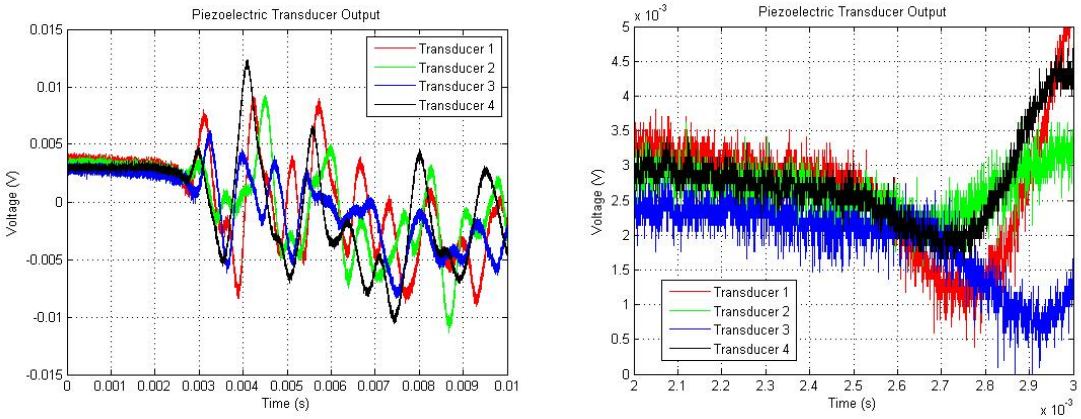

a) Unzoomed **b) Zoomed**

Figure 6. Piezoelectric transducer output.

transducers until the time of impact, which would allow the time of impact to be readily discerned.

In a laboratory environment, ambient background electrical and mechanical noise is relatively consistent and can be easily eliminated or mitigated through the use of shielding, filtering, or simple signal processing methods.

However, these approaches are not suitable for in-flight measurements due to the unpredictable nature of the noise sources. Mechanical vibration and flutter due to aerodynamic effects will vary considerably during flight, causing variances in the electrical output of the sensors. Piezoelectric devices and their associated wiring are also susceptible to electromagnetic interference. These sources all produce undesirable contributions to the total output of the sensors, often masking early indications of an impact which may be mistaken for noise using traditional signal processing techniques.

The data in Fig. 6 from the four sensors, acquired at a rate of 5 megasamples per second, illustrate the difficulty in identifying the arrival time of a signal resulting from an impact. Even in the zoomed graph (Fig. 6b), it is not readily apparent when the impact occurs, which leads to uncertainly in establishing the location of impact.

Digital filtering can help to reduce some of the noise, but does not eliminate the problem. Figure 7 shows a zoomed portion of a graph of the same signals after a 4th order Butterworth digital bandpass filter is applied with a lower cutoff frequency, f_1, of 80 Hertz (Hz) and a upper cutoff frequency, f_2, of 25 kHz, based on Fourier analysis of the signals. In addition to not aiding in identifying the time differentials, a further complication with using digital filtering for in-flight evaluation is that the choice of bandpass frequencies is dependent on current flight conditions. Spectral analysis of the signal can be used to identify the changes in the frequency response of the transducers, but at the expense of losing the temporal content necessary for determining the time differentials. Furthermore, Fourier transforms are suitable for representing infinite periodic sequences, but cannot adequately represent the finite, aperiodic signals characteristic of transient events.[6]

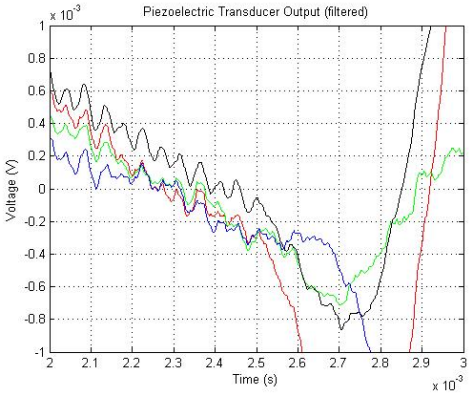

Figure 7. Filtered transducer output.

Wavelet transforms offer a more promising alternative to traditional signal processing methods.[7] These transforms allows for multiresolution analysis of a signal by decomposing that signal at multiple levels of detail and abstraction. These decomposed signals retain characteristics of the original signal in both the time and frequency domains simultaneously, so time differences in the signal outputs from the four piezoelectric transducers can be identified, despite changes in the spectral components of these signals caused by noise and aerodynamic effects.

With continuous Fourier transforms, signals are approximated in the frequency domain by a linear combination of sinusoids as given by Eq. (32). The inverse of this representation can be used to transform the signal back to the time domain (Eq. 33).

$$F(\omega) = \int_{-\infty}^{+\infty} f(t)\, e^{-i\omega t}\, dt \tag{32}$$

$$f(t) = \frac{1}{2\pi} \int_{-\infty}^{+\infty} F(\omega)\, e^{i\omega t}\, d\omega \tag{33}$$

In a similar manner, Ref. 8 shows a signal may be represented as a continuous wavelet transform by a linear combination of a basis function, ψ, known as a "mother wavelet," giving the wavelet coefficients W in Eq. (34), where ψ^* denotes complex conjugation. Unlike the sinusoidal Fourier transform, these functions are finite. A wavelet basis has compact support if the value of the function is zero outside of certain boundaries. This property of a wavelet with compact support was used for this application, since it allows wavelet transforms to retain the properties of the original signal in the time domain.

$$W(a,b) = \int_{-\infty}^{+\infty} f(t) \frac{1}{\sqrt{|a|}} \psi^* \left(\frac{t-b}{a} \right) dt \tag{34}$$

To simplify the notation, the expression $\psi_{a,b}$ is defined in Eq. (35) and the transform in Eq. (34) can be rewritten as Eq. (36).

$$\psi_{a,b}(t) = \frac{1}{\sqrt{|a|}}\psi\left(\frac{t-b}{a}\right) \tag{35}$$

$$W(a,b) = \int_{-\infty}^{+\infty} f(t)\,\psi^*_{a,b}(t)dt \tag{36}$$

The wavelet coefficients, *W*, are scaled and time shifted to represent the complete time spectrum at varying degrees of detail or abstraction.[8] The selection of the scale factor determines how much the signal is dilated ($a > 1$) or contracted ($0 < a < 1$). The time shift, *b*, determines which portion of the signal is transformed by the finite basis function. The exact values for *a* and *b* are both application dependent. The original signal can be completely reconstructed using the admissibility constant *C* derived from the Fourier transform of the wavelet function as given by Eqs. (37) through (39). However, by selectively setting some of the coefficients to zero, an approximation of the signal can be obtained without some of the undesirable noise which appears as detail in the wavelet transformation.

$$\Psi(\omega) = \int_{-\infty}^{+\infty} \psi(t)\, e^{-i\omega t}\, dt \tag{37}$$

$$C = \int_{-\infty}^{+\infty} \frac{|\Psi(\omega)|^2}{|\omega|} d\omega \tag{38}$$

$$f(t) = \frac{1}{C}\int_{a=-\infty}^{+\infty}\int_{b=-\infty}^{+\infty} \frac{1}{|a|^2} W(a,b)\,\psi_{a,b}(t)\,da\,db \tag{39}$$

For computer implementations, a discrete wavelet transformation can be used, which decomposes the signals into discrete levels, where *a* is equal to 2^n, with *n* representing the level of detail. Signals were transformed using the MATLAB Wavelet Toolbox[9] using the discrete form of Eqs. (34) through (39). Although there are many types of wavelet basis functions, biorthogonal wavelets are best suited for signal processing applications because of their compact support and linear phase property, allowing signals to be perfectly reconstructed without any phase shift.[10]

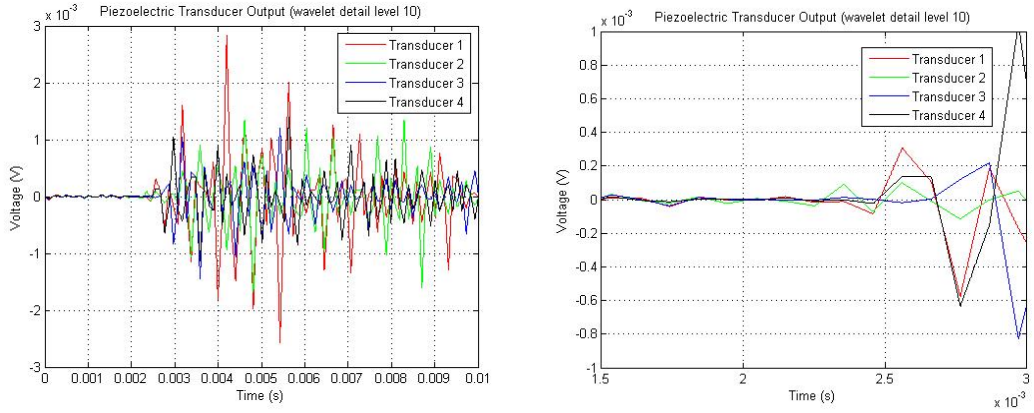

a) Unzoomed **b) Zoomed**

Figure 8. Piezoelectric transducer output reconstructed from wavelet detail level 10.

Figure 8 shows the signals from the four piezoelectric transducers as reconstructed using a discrete wavelet transform at the level of detail which maximized the signal (post-impact) to noise (pre-impact) ratio (S/N), which is computed in decibels (dB) using Eq. (40).

$$S/N = 10\log_{10}\frac{signal\ range}{noise\ range} \tag{40}$$

Table 1 shows the average signal to noise ratios for the unfiltered signals, the digitally filtered signals, and the signals reconstructed from a wavelet transform with a detail level of 10. In this case, level 10 was found to be optimum, resulting in a signal to noise ratio of 17.7 dB, a 12.4 dB increase over the filtered signal. Since this signal is reconstructed from a single level of detail, most of the noise in the original signal has been eliminated, allowing the time differentials to be more readily discerned (Fig. 8b).

Table 1. Signal to Noise Ratios.

	Unfiltered	**Filtered**	**Wavelet**
Signal range (V)	.0193	.0153	.00540
Noise range (V)	.00781	.00451	.0000916
S/N (in dB)	3.9	5.3	17.7

V. Identifying Time of Impact Using a Neural Network

For in-flight assessment of a foreign object impact, signals from the piezoelectric sensors must be analyzed to determine if an impact has occurred. The first step towards identification of an impact involves a simple threshold technique to ascertain if the measured value from the sensors significantly exceeded the background noise level. This assessment is easily performed at the time of acquisition by establishing an analog voltage trigger level. When the received signal exceeds this threshold, the recording of the signal begins, including a portion of the pretrigger data for the determination of the time differentials as previously discussed.

Accurately determining the location of impact depends on the determination of these time differentials. This in turn relies on the ability to determine the earliest time at which the signal has changed as a result of the impact. To make this determination, the reconstructed signal from Eq. (38) is segmented into small time regions, and the signal from that region is processed by a trained neural net to determine if it indicates the start of an impact. Portions of the signal which are not associated with the impact will exhibit degrees of consistency across the time segment, whereas those portions indicative of an impact will contain evidence of discontinuity within the segment. The signal was segmented into these regions, with a 50% overlap in the segments to ensure that at least one segment completely contains data associated with the measurement of the moment of impact.

Artificial neural networks have been proven effective for impact detection.[11] Neural networks transform measured inputs into expected outputs using a set of weights and are computationally efficient after training.[12] The outputs are a linear combination of these inputs and the weights. The network is "trained" using supervised learning by adjusting the weights such that the error (the actual output of the network compared to the expected output) is locally minimized. A multilayer feed-forward neural network[13] was used consisting of 24 inputs, a single hidden layer of four nodes, and a single output. The segmented inputs were obtained from the reconstructed signals and further condensed into 24 inputs by averaging. The choice of 24 nodes was a tradeoff between maximizing accuracy and minimizing execution time. The number of nodes in the hidden layer was chosen experimentally to be small enough to facilitate learning without being so large as to memorize the patterns used for training[13], which would impede the network from recognizing patterns not already present in the set of data used to train the network. The single output was a measure of the likelihood that this segment indicated the detection of an impact.

The output from the neural network served two purposes. First, the network aided in determining if an impact occurred at all by examining each segment of the received signal. Second, if the determination was that an impact had occurred, the neural network helped identify in which time segment the impact was first detected. That segment was further examined to determine the point in time when the impact occurred.

The output of the net is the weighted, biased sum of all the inputs, adjusted by an activation function to restrict the output between a range of values. The output of a node is given by the sum of the weights associated with that node. The error associated with the output of the network can be computed as the mean square error based on the differences between the actual outputs of the network and the expected outputs used for training. The network is trained by adjusting the weights to minimize the total Mean Squared Error (MSE).[13]

The neural network was constructed and trained using the Neural Network Toolkit for MATLAB.[14] The Levenberg-Marquardt method was used to train the network because of the reduced learning time associated with higher-order training methods.[15] Sets of data collected from all four sensors from 35 impacts yielded a total of 140 signals. An additional 35 sets of data were collected when no impact occurred. Both the impact and non-impact

signals were segmented and used to train and validate the network. Eighty percent of the data were used to train the network, with the remaining 20% reserved for simulation and testing of the trained network. The network was trained using repeated training runs, and in all but two runs, the network was able to converge below the target error level (less than .001 MSE) within 3000 cycles, or epochs. Neural networks frequently do not converge because of the initial value of the weights, which are randomly initialized to avoid biasing the output of the network.[16]

VI. Results and Conclusion

The use of coordinate transformations to scale the location of the sensors relative to a unit square simplified the determination of the point of impact, but did require the extra step to transform these relative coordinates back into the test coordinate system. The location of impact was able to be determined using piezoelectric sensors, but the ability to determine the location of impact was greatly dependent on the accurate determination of the differences between the times that the impact was identified at each sensor.

These time differentials were difficult to identify using only digital filtering because of the low signal to noise ratios as shown in Table 1 (5.3 dB). Using wavelet transforms for multiresolution analysis resulted in a signal to noise ratio of 17.7 dB. Wavelet analysis was 12.4 dB more effective at noise reduction than with traditional Fourier analysis and digital filtering, allowing the time differentials to be determined with greater accuracy.

The neural network aided in the identification of the time differentials by pattern matching to determine if a segment of the signal is consistent throughout the segment, or if there is a change in the signal indicative of the detection of an impact. The neural network correctly identified the segment of the signal that included the impact 93% of the time. The accuracy would likely have been greater had more test cases been used to train the neural net. The ability of a neural network to adapt to changing conditions by retraining makes it well-suited for in-flight impact detection.

Even small errors in the arrival times of the signals resulting from the impact can result in significant errors in the computed location of the impact. These errors in the location of impact can be greater than the error in the time differentials by an order of magnitude or more, as shown in section III of this paper. Using the techniques presented in this paper, the 12.4 dB gain in signal to noise ratio allows the arrival times of the signal at each sensor to be readily distinguished.

References

[1]Prosser, W. H., "Development of Structural Health Management Technology for Aerospace Vehicles," *Joint Army, Navy, NASA, Air Force (JANNAF) 39th Combustion Subcommittee Meeting*, 2003.

[2]Guirgiutiu, V., and Cuc, A., "Embedded Non-destructive Evaluation for Structural Health Monitoring, Damage Detection, and Failure Prevention," *The Shock and Vibration Digest*, Vol. 37, No. 2, 1985, pp. 83-105.

[3]Coverly, P. T., and Staszewski, W. J., "Impact Damage Location in Composite Structures Using Optimized Sensor Triangulation Procedure," *Smart Materials and Structures*, Vol. 12, 2003, pp. 795-803.

[4]Lin, M., Qing, X., Kumar, A., and Beard, S. J., "SMART Layer and SMART Suitcase for Structural Health Monitoring Applications," *Proeedings of the International Society for Optical Engineering (SPIE)*, Vol. 4332, 2001, pp. 98-106.

[5]MATLAB Ver. 7.1.0.246 (R14), The MathWorks, Natick, MA, 2005.

[6]Graps, A., "An Introduction to Wavelets," *IEEE Computational Science and Engineering*, Vol. 2, No. 2, 1975, pp. 1-18.

[7]Kim, I.-G., Lee, H.-Y., and Kim, J.-W., "Impact Damage Detection in Composite Laminates Using PVDF and PVT Sensor Signals," *Journal of Intelligent Material Systems and Structures*, Vol. 16, 2005, pp. 1112-1118.

[8]Rao, R. M., and Bopardikar, A. S., *Wavelet Transforms: Introduction to Theory and Applications*, Addison Wesley Longman, Reading, MA, 1998, Chap. 1.

[9]Mallat, S. "A Theory for Multiresolution Signal Decomposition: The Wavelet Representation," *IEEE Transaction on Pattern Analysis and Machine Intelligence*, Vol. 2, No. 7, 1989, pp. 674-693.

[10]Misiti, M., Misiti, Y., Oppenheim, G., and Poggi, J.-M., *Wavelet Toolbox User's Guide*, The MathWorks, Natick, MA, 1996, Chaps. 1-3.

[11]Staszewski, W. J., Worden, K., Wardle, R., and Tomlinson, G. R., "Fail-Safe Sensor Distributions for Impact Detection in Composite Materials," *Smart Materials and Structures*, Vol. 9, 2000, pp. 298-303.

[12]Rumelhart, D. E., and McClelland, J. L., *Parallel Distributed Processing: Explorations in the Microstructure of Cognition*, Vol. 1, MIT Press, Cambridge, MA, 1986.

[13]Hagan, M. T., Demuth, H. B., and Beale, M., *Neural Network Design*, PWS Publishing Company, Boston, MA, 1996, Chaps. 11, 12.

[14]Demuth, H., and Beale, M., *Neural Network Toolbox User's Guide*, The MathWorks, Natick, MA, 2000, Chap. 5.

[15]Shepherd, A. J., *Second-Order Methods for Neural Networks*, Springer-Verlag, London, 1997, Chap. 3.

[16]Reed, R. D., and Marks II, R. J., *Neural Smithing: Supervised Learning in Feedforward Artificial Neural Networks*, MIT Press, Cambridge, MA, 1999, Chap. 7.